Quantification of β-adrenoceptor density in the human heart with (*S*)-[^{11}C]CGP 12388 and a tracer kinetic model

Petra Doze, Philip H. Elsinga, Aren van Waarde, Remge M. Pieterman, Jan Pruim, Willem Vaalburg, Antoon T.M. Willemsen

PET Center, Groningen University Hospital, P.O. Box 30001, 9700 RB Groningen, The Netherlands

Received 3 September and in revised form 1 November 2001 / Published online: 19 January 2002

Abstract. The aim of this study was to determine whether the β-adrenoceptor receptor density (B_{max}) and the ligand affinity (K_D) of (*S*)-[^{11}C]CGP 12388 for the β-adrenoceptor receptor could be determined using full tracer kinetic modelling of the transport of the ligand and its interaction with the receptor. This approach minimises the a priori assumptions and may thus serve as a gold standard to validate other simplified methods. Dynamic positron emission tomography (PET) data were acquired in six healthy subjects during 60 min. Three different injection protocols were applied, each consisting of three injections with varying SAs: high specific activity (SA), low SA or unlabelled ligand only. Arterial blood samples were collected via a cannula in the radial artery. Time-activity data in myocardial tissue were obtained using regions of interest (ROIs) on short-axis planes. All data were analysed with a two-tissue compartment, six-parameter (K_1, k_2, k_{on}, k_{off}, B_{max}, F_{bv}) model that relies on explicit compartments for describing the kinetics of both labelled and unlabelled radioligand. Time-activity curves showed that unlabelled ligand could displace the radioligand from the receptor. This resulted in increased radioactivity levels in plasma. Modelling results yielded B_{max} values of 9.74±1.80 n*M* and a K_D of 0.58±0.22 n*M*, assuming a reaction volume of 0.15. In addition, parametric polar images of B_{max} could be calculated. The protocol with injections of high SA, low SA, and unlabelled ligand, respectively, was found to be the most sensitive to parameter changes. We conclude that with tracer kinetic modelling of (*S*)-[^{11}C]CGP 12388, the β-adrenoceptor density in the human heart can accurately be obtained in vivo. This approach may thus serve as a gold standard.

Antoon T.M. Willemsen (✉)
PET Center, Groningen University Hospital, P.O. Box 30001, 9700 RB Groningen, The Netherlands
e-mail: a.t.m.willemsen@pet.azg.nl
Tel.: +31-50-3613311, Fax: +31-50-3611687

Keywords: β-Adrenoceptor – PET – Tracer kinetic model – Receptor density

Eur J Nucl Med (2002) 29:295–304
DOI 10.1007/s00259-001-0714-0

Introduction

Positron emission tomography (PET) is an excellent tool for investigation of the distribution of various receptors in vivo in humans. However, the real challenge of studying ligand-receptor interactions with PET is the quantitative analysis of the pharmacokinetics and pharmacodynamics of a radioligand in vivo, in order to assess receptor densities and the affinity of a ligand for a particular binding site. This pharmacological information allows us to study receptor densities in normal and pathological conditions, to monitor the effect of medical interventions and to investigate the interaction of unlabelled drugs with the receptor.

The β-adrenergic receptor density in the human heart is altered in various pathophysiological conditions, including hypertension, heart failure, ischaemia and hypertrophic and dilated cardiomyopathy (HCM, DCM) [1]. Quantification of myocardial and pulmonary β-adrenoceptors with PET is therefore likely to become a powerful tool by which to investigate β-adrenoceptor changes during the course of these diseases and to monitor the effects of treatment [2].

β-Adrenoceptor densities have already been determined with PET in healthy volunteers and patients with HCM or DCM [3, 4] or asthma [5], using the hydrophilic β-adrenoceptor antagonist (*S*)-[^{11}C]CGP 12177. In these studies, the B_{max} was calculated in a two-injection protocol [high and low specific activity (SA)], using a graphical method [6]. We prefer to quantify B_{max} and K_D with a tracer kinetic model since, in principle, this allows the identification of all model parameters while requiring only standard a priori assumptions. In contrast, other

simplified models, including the graphical model, are based on many additional hypotheses and often allow only the identification of composites of parameters (e.g. B_{max}/K_D, rather than B_{max}). For this study, (*S*)-CGP 12388, the isopropyl analogue of (*S*)-CGP 12177, was used since it produces excellent PET images of heart, lung and spleen, it is equally potent and its synthetic procedure is more suitable in a clinical setting than the multistep synthesis of (*S*)-[^{11}C]CGP 12177 from [^{11}C]phosgene [7].

Tracer kinetic models are designed to give a simplified description of the behaviour of a (radio)ligand in the living body. In a standard two-tissue compartment model for receptor binding, first proposed by Mintun et al. [8], the tissue compartments represent free radioligand in tissue and receptor-bound radioligand, where the input function is represented by the free radioligand concentration in plasma. The transfer coefficients K_1 and k_2 represent the exchange between blood and tissue, while k_3 and k_{off} describe receptor association and dissociation (Fig. 1). In principle, all parameters can be identified from a dynamic PET scan using non-linear least squares optimisation, which yields an equation/curve that best describes the data.

B_{max} can be calculated from $k_3=(k_{on}/V_R)\times(B_{max}-B)$, where B represents the amount of ligand that is bound to the receptor. However, for measurements with a tracer dose it follows that $B<<B_{max}$ and thus only the combination $(k_{on}/V_R)\times B_{max}$ can be determined. Therefore, high and low SA measurements (preferably in a single experiment) must be combined if a unique solution for B_{max} is required. Careful optimisation of the injection times and SAs can improve the accuracy not only of B_{max} but also of the other model parameters [9, 10]. Once such a complex model has proven its value, it may serve as a gold standard during the optimisation and development of simplified experimental procedures, such as the graphical method, that can be applied for routine patient studies.

The aim of this study was to determine whether tracer kinetic modelling of (*S*)-[^{11}C]CGP 12388 PET data can yield all model parameters, and in particular the β-adrenoceptor density and the ligand affinity, in the myocardium of healthy volunteers.

Materials and methods

Preparation of (S)-[11C]CGP 12388. (*S*)-[^{11}C]CGP 12388 was prepared as described previously by reductive alkylation of the (*S*)-desisopropyl precursor with [^{11}C]acetone [11]. (*S*)-[^{11}C]CGP 12388 was purified on an Econosphere C-18 column with saline and 20 m*M* NaH_2PO_4/ethanol 88/12 (v/v) as mobile phase. The flow rate was 5 ml/min. The end-product was diluted to an ethanol percentage <10% and passed through a Millipore GP (0.22 µm) filter. Total synthesis time was 38 min. The overall radiochemical yield and SA were 10%–20% EOB and 19–102 MBq/nmol EOB, respectively.

Human volunteers. Healthy volunteers were recruited using the following inclusion criteria: age 18–65 years, willingness to cooperate and to sign an informed consent form, declared healthy after medical examination (including screening for normal kidney and liver function). Exclusion criteria were: a positive history regarding myocardial ischaemia, hypertension, heart failure, angina, wheezing or tightness of the chest related to asthma or chronic obstructive pulmonary disease, or infections of the upper respiratory tract within the 4 weeks prior to the study, use of β-mimetics (salbutamol) or theophylline (≤12 and 48 h, respectively) prior to the study, and, for females, pregnancy or possible pregnancy. The study was approved by the Medical Ethics Committee of Groningen University Hospital. Each subject was informed about the purpose and hazards of the experiment both orally and in writing, and gave informed consent. Subject information (sex, age and weight) is shown in Table 1.

Before the study, a cannula was placed in a vein of one of the lower forearms. Another cannula was placed in the radial artery of the contralateral arm, after patency of the ulnar artery had been proven by the Allen test. The arterial cannula was inserted under local anaesthesia with lidocaine. The venous cannula was used for injection of the radioligand and the arterial line for blood sampling.

Study protocol. The volunteer was placed in the PET camera (Siemens/CTI ECAT 951/31, FWHM =6 mm) in the supine position. A rectilinear scan was made for proper positioning (including the heart, lung and spleen within the field of view). Arterial blood pressure and electrocardiograms were monitored throughout the experiment. To correct for attenuation, a transmission scan of 20 min was performed, using the internal ^{68}Ge/^{68}Ga sources.

Three different injection protocols were applied, each consisting of three injections with varying SAs. The first injection always contained (*S*)-[^{11}C]CGP 12388 with high SA (SA at T_0 =19.4–49.8 MBq/nmol). The second and third injections, administered 20 and (approximately) 40 min later, contained either radioligand in low SAs or non-radioactive ligand only. In Table 1 the exact time of injection, amount of radioactivity and SA of each injection in the different protocols are shown. In experiments using three radioactive injections (volunteers 1 and 2, Table 1), a second radiosynthesis was necessary for the third injection. All injections were administered over a period of 1 min using a Medrad OP-100 remote-controlled pump (Medrad, Indianola, Pa.) and after each injection the lines were flushed with saline to ensure complete delivery of the radioligand.

Data acquisition. Data acquisition was started at the onset of the first injection. Two different acquisition protocols were used. In both protocols the sequence of frame rates was repeated after each injection, yielding a total acquisition time of 60 min. For volunteers 1–4 a frame rate of 6×10 s, followed by 2×30 s, 2×1 min, 2×2 min and 4×3 min was applied (3 times). To gain more information about the behaviour of the (radio)ligand immediately after injection, a more extensive acquisition protocol was used for volunteers 5 and 6: 12×10 s, 2×30 s, 1×1 min, 2×2 min and 4×3 min (3 times).

Arterial blood samples (2 ml) were drawn at 0.5-min intervals during the first 5 min and at 10-min intervals from 10 to 20 min after each injection. The radioactivity in plasma (250 µl, obtained by centrifugation at 3,000 *g* for 5 min) and whole blood (250 µl) was determined using a gamma counter (LKB Wallac CompuGamma 1282 CS, Turku, Finland) which was cross-calibrated with the PET camera. Radioactivity in the cellular fraction was

Table 1. Study information for the six volunteers and numerical values of the study protocol

		Volunteer					
		1	2	3	4	5	6
Information	Age (years)	25	24	41	50	25	46
	Sex	M	F	M	M	F	F
	Weight (kg)	69	66	88	64	65	73
First injection (T_0)	SA (MBq/nmol)	34.9	49.8	21.7	36.8	24.2	19.4
	Activity (MBq)	194.7	119.5	201	218	201	201
	Mass (nmol)	5.6	2.4	9.3	5.9	8.3	10.3
Second injection	T_1 (min after T_0)	20	20	20	20	20	20
	SA (MBq/nmol)	34.9	49.8	21.7	36.8	24.2	0
	Activity (MBq)	390.4	217.9	394.8	388.9	434	0
	Mass (nmol)	11.2	4.4	18.2	10.6	17.9	0
	Additional mass (nmol)	81	77	105	66	62	270
Third injection	T_2 (min after T_0)	45.5	54.5	40	40	40	40
	SA (MBq/nmol)	94.9	102.1	0	0	0	19.4
	Activity (MBq)	907.1	1517.6	0	0	0	429
	Mass (nmol)	7.9	9.1	0	0	0	23.7
	Additional mass (nmol)	318	300	405	294	300	248

SA (specific activity) and activity are given at T_0

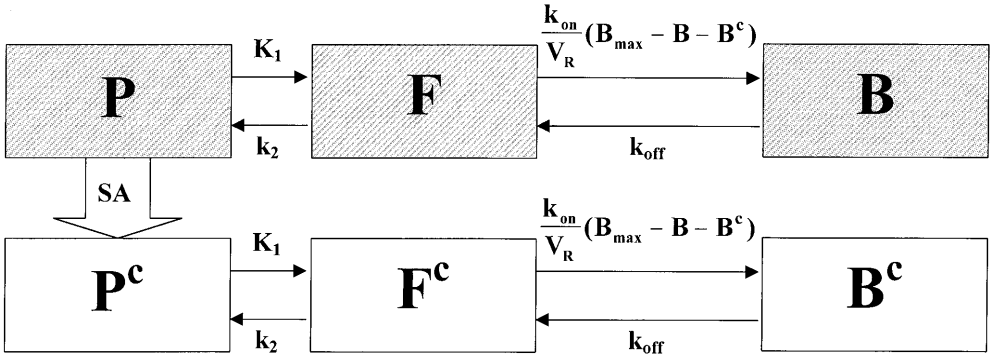

Fig. 1. Schematic representation of a tracer kinetic model incorporating explicit compartments for both labelled and unlabelled radioligand. Compartments represent the possible states of the ligand: in plasma (*P*), free in tissue (*F*) and bound to receptors (*B*). *Cross-hatched* and *open boxes* represent hot and cold ligand concentrations, respectively. The superscript c refers to unlabelled (cold) ligand. First-order rate constants (K_1, k_2, k_3, k_{off}) describe the transition of ligand between different compartments. The SA is used to generate a plasma input function for unlabelled ligand from the plasma input of labelled ligand

calculated using plasma and whole blood data, in combination with the measured haematocrit value. Radioactivity data were automatically corrected for dead time and decay.

Data analysis. For the data analysis of myocardial tissue, emission scans (transaxial planes) were re-oriented into ten short-axis images, from the base of the heart to the apex. For analysis of the whole left ventricle, several frames of the short-axis images, acquired at the end of the first injection, were summed to produce high-contrast images on which the regions of interest (ROIs) were drawn. ROIs were drawn on the whole of the left ventricle in three different planes and grouped together, yielding a single time-activity curve.

For parametric polar map analysis (volunteers 3–6), each short-axis image was divided into 12 segments, using a fully automatic non-operator-dependent program based on MATLAB (The Mathworks, Inc., Natick, Mass.).

The mean tracer activity in all ROIs or polar map regions was calculated (MBq/ml), after correction for ^{11}C decay, and plotted against time using ECAT software (CAPP7.1, CTI/Siemens, Knoxville, Tenn.), running on a SUN/SPARC workstation. Parametric polar maps of B_{max} values were smoothed using a two-dimensional gaussian filter.

Compartmental model. The compartmental model used in this study, as shown in Fig. 1, is a non-equilibrium, non-linear model based on the work of Delforge et al. [6, 9, 12]. It allows for the calculation of the B_{max} and the K_D values. This model relies on explicit compartments for description of the kinetics of both labelled and unlabelled radioligand. In this study, the model contained four tissue compartments and six unknown parameters (Fig. 1). First order rate constants (K_1, k_2, k_3, k_{off}) describe the transition of li-

gand between different states. K_1 is presented in ml ligand/min per ml tissue while the other rate constants are presented in min^{-1}. The rate constant k_3 is not a proper constant but rather depends on the available binding sites during the experiment; $(k_{on}/V_R)\times(B_{max}–B–B^c)$. Here k_{on} [in ml/(min×pmol)] is the ligand-receptor association constant, while V_R represents the reaction volume. The concentration of available free receptors is given by $(B_{max}–B–B^c)$ in pmol/ml, with B and B^c being the concentration of bound receptors due to the labelled and the unlabelled ligand, and B_{max} the total concentration of receptors, as discussed above.

Because of the limited resolution of the PET camera and the internal heterogeneity of the tissue, the true *local* free ligand concentration is unknown. Therefore, the denominator V_R was introduced to account for the heterogeneity of the free ligand concentration [13]. The parameter k_{on}/V_R is called the macroscopic association rate constant and corresponds to the association constant measured with PET. Since (*S*)-CGP 12388 is a hydrophilic molecule (log P=–0.6, [11]), its V_R should be close to the fraction of extracellular fluid in tissue, resulting in a V_R of 0.15 [14].

The differential equations for describing the concentrations of both labelled (hot) and unlabelled (cold) ligand in the different compartments are:

$$\frac{dF}{dt} = K_1 C_p(t) - k_2 F - \frac{k_{on}}{V_R}\left[B_{max} - B - B^c\right]F + k_{off}B \quad (1)$$

$$\frac{dB}{dt} = \frac{k_{on}}{V_R}\left[B_{max} - B - B^c\right]F - k_{off}B \quad (2)$$

$$\frac{dF^c}{dt} = K_1 C_p^c(t) - k_2 F^c - \frac{k_{on}}{V_R}\left[B_{max} - B - B^c\right]F^c + k_{off}B^c \quad (3)$$

$$\frac{dB^c}{dt} = \frac{k_{on}}{V_R}\left[B_{max} - B - B^c\right]F^c - k_{off}B^c \quad (4)$$

where C_p, F and B represent the concentrations of the ligand in plasma, free in tissue and bound to receptors, respectively (pmol/l). The superscript c refers to unlabelled (cold) ligand. Note that the models for the labelled and unlabelled ligand are coupled through the effective association rate $(k_{on}/V_R)\times(B_{max}–B–B^c)$. In practice, $B<<B^c$ so this association rate reduces to $(k_{on}/V_R)\times(B_{max}–B^c)$.

Solving these differential equations gives the simulated free and bound concentrations of both labelled and unlabelled ligand. For a given blood volume (F_{bv}), the final PET signal can then be calculated from the following equation:

$$PET_{i+i} = \frac{1}{t_i + i - t_i}\int_{t}^{t_{i+1}} \left[F_{bv}C_{BL} + (1 - F_{bv})(F + B)\right] dt \quad (5)$$

with C_{BL} the concentration of ligand in blood.

Arterial input function. The concentration of hot ligand in plasma (C_p) was assessed by blood sampling during the experiment. The plasma data of the first and second injections were extrapolated to 60 min and subtracted from the measured plasma activity to yield the net radioactivity in plasma after the second and third injections. This hot input function was applied to generate a plasma input function for unlabelled ligand, using the SA of each radioligand injection (indicated by the *arrow* in Fig. 1). When an injection consisted of unlabelled ligand only, the corresponding unlabelled plasma curve was obtained by linear scaling and displacing the plasma curve resulting from the first injection.

Parameter estimation. Due to the non-linear association rate $[(B_{max}–B^c)F$ and $(B_{max}–B^c)F^c)]$ the differential equations (Eqs. 1–4) must be solved numerically. This was achieved using a multistep variable-order ordinary differential equations solver.

To calculate and minimise the error between simulated and measured PET signal, a non-linear (weighted) least squares optimisation was applied, according to the interior-reflective Newton method [15, 16]. Weighting was based on the measured total counts rather than count rate, taking into account the decay correction of the PET data. The estimation of the uncertainties in the model parameters was performed according to Millet et al. [17]. All calculations were performed in MATLAB (The Mathworks, Inc., Natick, Mass.). For more details see, for example, [9] and [18].

The optimisation routine employs the gradients of the error functions. To prevent instability due to numerical differentiation, the gradients were also calculated by the ODE solver. Since $\partial/\partial p_i(\partial PET/\partial t)=\partial/\partial t\,(\partial PET/\partial p_i)$, with p_i one of the model parameters, it is obvious that the required gradients themselves can be written as a system of differential equations. This resulted in 20 additional differential equations, which were calculated simultaneously with the original four equations for the model itself. As the ODE servers are generally most efficient when combined with the Jacobian, the 24 by 24 sparse Jacobian matrix was also determined and supplied to the ODE solver. Optimisation took between 1 and 5 min (SUN UltraSparcII, 250 MHz) depending on the quality of the data and the fit starting values.

Sensitivity. The sensitivity of the fits for changes in the model parameters can be determined from the partial derivatives. These in turn can be calculated numerically by finite differencing. For display purposes the response due to the consecutive perturbation by +10% or –10% of the optimal parameters, determined previously using non-linear least square fitting as described above, was also calculated.

Results

Time-concentration curves

All protocols could be reliably completed within 1 1/2 h. In Fig. 2 an example of a time-concentration curve (solid line) is shown, which was obtained from an ROI drawn on myocardial tissue from the whole left ventricle (mean of three planes in volunteer 4).

After the first injection of (*S*)-[^{11}C]CGP 12388 with a high SA, apparent tissue levels of radioactivity rose to a maximum, mainly due to spill-over from the blood pool (see also Fig. 4), followed by a relatively slow decline, reaching a plateau within 3 min. The subsequent injection of radioligand with low SA (volunteers 1–5) at 20 min also resulted in a very rapid rise in activity, followed by a rapid decline (0.71±0.58 min^{-1}). Radioactivity continued to decrease slightly (0.012±0.006 min^{-1}), indicating dissociation of the labelled ligand from the re-

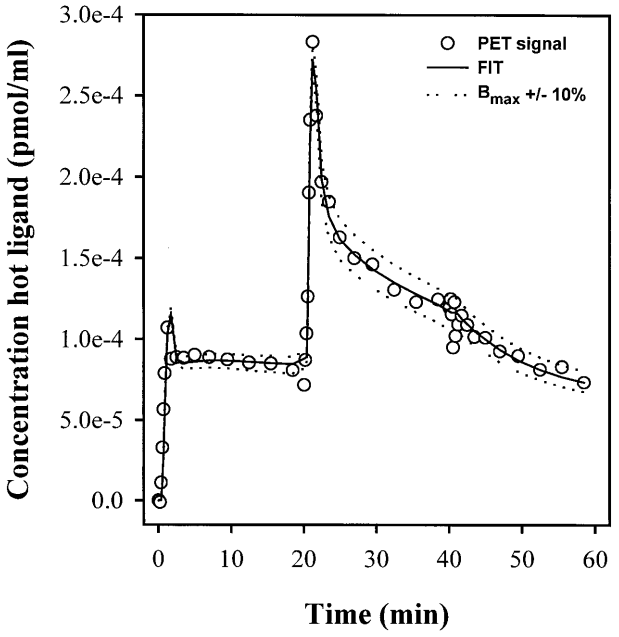

Fig. 2. Measured PET signal (○) and the simulated fit (*solid line*) of volunteer 4 for a large region of the left ventricle. The *dotted lines* represent the simulated response when B_{max} was set at ±10% of the optimal value

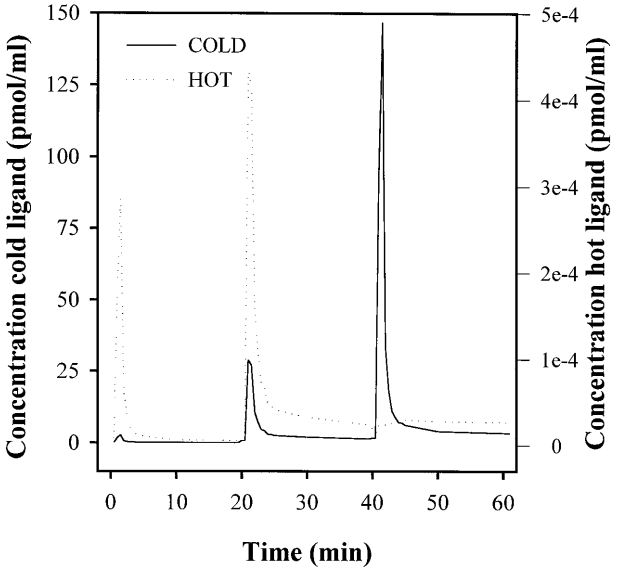

Fig. 3. Time-concentration curves of labelled (hot) and unlabelled (cold) ligand obtained in plasma of volunteer 4

ceptor. The third injection at 40 min p.i., consisting of unlabelled ligand only (volunteers 3–5), resulted in a further decline in radioactivity (exponential decline: 0.22±0.07 min^{-1}).

Volunteers 1 and 2 received a co-injection of labelled and unlabelled ligand at 40 min, with a lower SA than the second injection. This third injection produced a fast rise in radioactivity, comparable to that after the second injection.

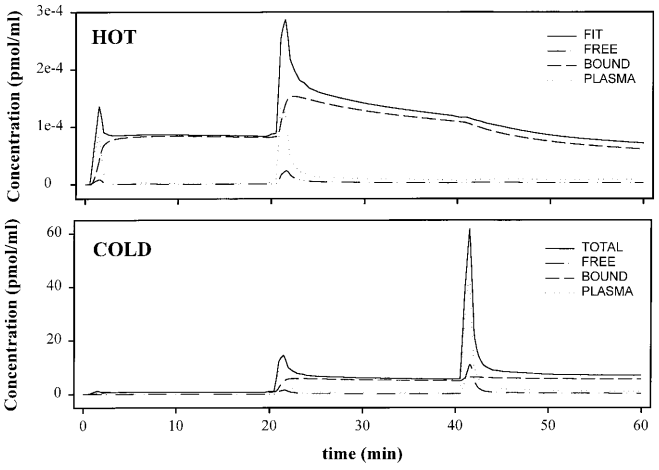

Fig. 4. Simulation of the PET signal obtained in the whole left ventricle of volunteer 4, and the corresponding labelled (hot) and unlabelled (cold) ligand concentrations in each compartment. All concentrations are corrected for blood volume

In volunteer 6, the second injection contained unlabelled ligand only. This resulted in an immediate decrease in labelled ligand comparable with the effect of the third injection in volunteer 4, as shown in Fig. 2. The results after the third injection in this volunteer resembled those obtained after the second injection of all other experiments. In plasma, after injections containing unlabelled ligand only, radioactivity levels rose slightly (see third injection in Fig. 3), as a result of the displacement of labelled ligand from the receptor.

Figure 4 (upper graph) depicts the estimates of the blood, free and bound concentrations of the labelled ligand (in volunteer 4), all corrected for blood volume, constituting the PET signal as defined in Eq. 5. The lower graph of Fig. 4 shows the corresponding concentrations for the unlabelled ligand, also corrected for blood volume. The concentrations of ligand in blood and free in tissue, both labelled and unlabelled, resembled those observed in plasma, as depicted in Fig. 3. The concentration of labelled ligand that was bound to receptor sites followed the measured PET signal, but was slightly lower. Clearly, unlabelled ligand displaced the hot ligand from the receptor sites. The fraction of unlabelled ligand that was bound to the receptors increased slightly after co-injection or injection of unlabelled ligand, reaching a plateau after 3 min (lower graph in Fig. 4). Although the third injection contained more mass than the second one (Table 1; volunteer 4), the calculated rise of unlabelled bound ligand was not as high as after the second injection.

Figure 5 depicts the occupancy of the receptors by the ligand over time. After the first injection only ca. 10% of the receptors were occupied by the ligand. After the second injection with low SA (see Table 1) already ca. 80% of the receptors are occupied. A third injection with even lower SA, occupies only ca. 10% more of the receptors.

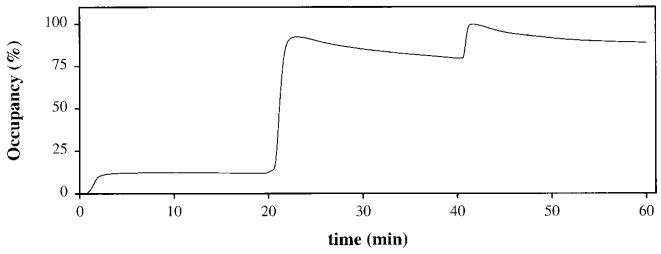

Fig. 5. β-Adrenoceptor occupancy after three injections of (*S*)-[^{11}C]CGP 12388 in volunteer 4

Table 2. Tracer kinetic parameters of (*S*)-[^{11}C]CGP 12388 in the left ventricle

Volunteer	K_1	k_2	k_{on}/V_R	k_{off}	B_{max}	bv	K_D
1	0.97	5.39	0.44	0.05	8.12	0.21	0.69
2	0.60	5.39	1.12	0.14	10.37	0.32	0.81
3	0.52	5.01	1.05	0.07	10.74	0.37	0.42
4	0.70	5.66	0.96	0.05	9.19	0.31	0.37
5	0.84	7.53	1.27	0.07	7.51	0.27	0.38
6	0.92	5.17	1.69	0.21	12.5	0.44	0.83
Mean	0.76	5.69	1.09	0.10	9.74	0.32	0.58
SD	0.18	0.93	0.41	0.06	1.80	0.08	0.22

Values for K_1 are given in ml ligand/min per ml tissue, k_{on}/V_R in ml/(min×pmol), k_2 and k_{off} in min^{-1}, and B_{max} in n*M*. The affinity (K_D in n*M*) is calculated by $(k_{off}/k_{on}/V_R)/V_R$, assuming that V_R=0.15. bv, Blood volume in the ROI

Identification of model parameters

Individual estimates in the whole left ventricle of all kinetic parameters are presented in Table 2. B_{max} values of 9.74±1.80 n*M* and K_D values of 0.58±0.22 n*M* were calculated, assuming a reaction volume of 0.15. No systematic differences were observed between the different injection protocols, when considering the parameter values. Omitting the data from the third injection in volunteers 3–5 changed the receptor density by –3%, –8% and 6%, respectively, while K_D values were changed by –11%, –14% and –6%, respectively. The plasma peak activity may be underestimated owing to undersampling in the first minutes after the injections. To assess the effect of this potential underestimation, plasma peak values were increased by 20% and the optimisation was repeated. This had little effect on the parameters; for example, B_{max} changed by –4%±2%.

Data analysis with parametric polar maps displayed a heterogeneous distribution of the estimated B_{max} values in the left ventricle; in all volunteers the receptor densities appeared to be higher in the inferior part of the left ventricle than in the anterior part. Figure 6 shows the distribution of B_{max} in volunteer 4. The mean B_{max} obtained from the 120 segments amounted to 8.65±3.15 (mean±SD for volunteers 3–6).

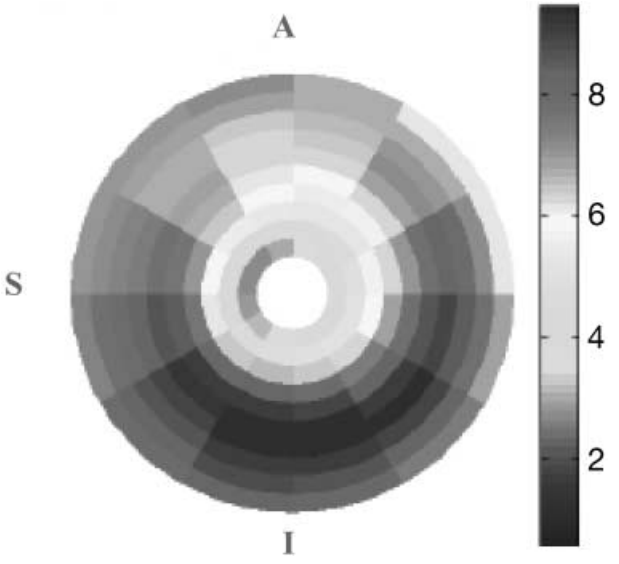

Fig. 6. Polar map of volunteer 4, demonstrating the regional distribution of B_{max}. *A*, Anterior; *S*, septal; *I*, inferior. Mean B_{max}= 6.71±1.70

Sensitivity

The simulated PET response was sensitive to a 10% change in the B_{max}, especially after the second and third injections (Fig. 2), showing differences of up to 9%–10%. As expected, perturbing K_1 by 10% changed the response by 7% (average blood volume of 30%). Changing the other parameters by 10% had much less effect on the fit (data not shown). The second protocol (high SA – low SA – unlabelled) was most sensitive to 10% changes in the B_{max}, while the third protocol (high SA – unlabelled – low SA) was totally insensitive to these changes.

Function of SA over time

The log SA was plotted for plasma and the two tissue compartments to see how the SA of the compartments differed over time (Fig. 7; volunteers 4 and 6). The first injection resulted in constant high SA levels. The second injection in volunteer 4 (low SA) lowered the SA in particular in plasma and the free compartment. Addition of unlabelled ligand only (40 min in volunteer 4) lowered the SA in plasma and the free compartment very rapidly to a minimum, after which it increased again, probably eventually reaching an equilibrium (after 70 min). The SA of the bound compartment also decreased but much more slowly, and without the rapid decline to a minimum.

When the second and third injections were reversed (volunteer 4 vs volunteer 6), the behaviour of the SA was also reversed. The low SA injection at 40 min increased all the SA values but most rapidly and most

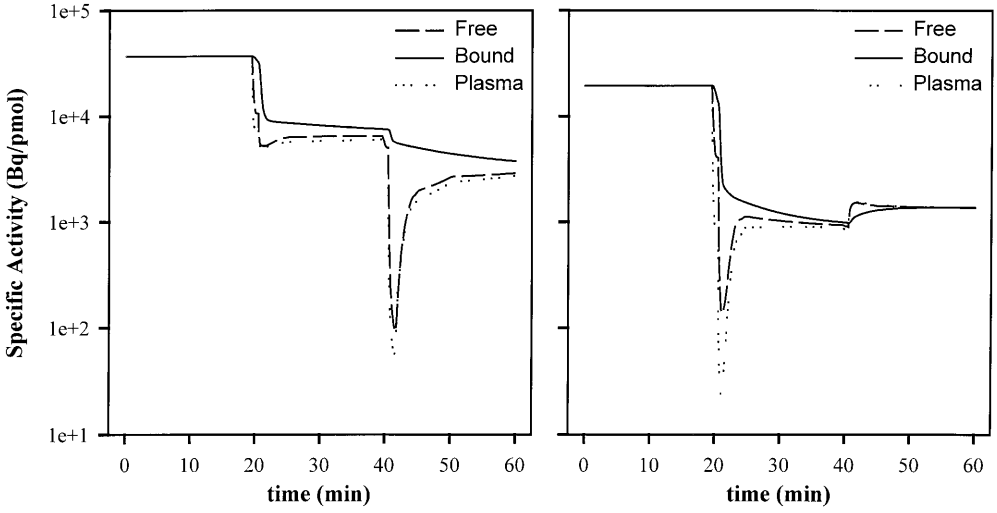

Fig. 7. Change in SA over time in each compartment, using different injection protocols; high SA – low SA – unlabelled (volunteer 4) on the *left* and high SA – unlabelled – low SA (volunteer 6) on the *right*

markedly in plasma and the free compartment, with an apparent equilibrium state being reached after only 10 min. The bound compartment was not as sensitive to the change in SA and increased more slowly, but also reached an equilibrium after 10 min.

Discussion

Protocol selection

As shown above, multiple injections at different SAs are essential for the accurate assessment of the B_{max}. Two injections (a tracer dose, followed by unlabelled ligand to occupy the receptor) might be sufficient in some studies. Delforge et al., however, showed that for [^{11}C]MQNB, a double-injection protocol may not provide a unique solution, although the simulated PET data resembled the total signal rather well. Therefore, these researchers suggested that initially three injections are needed (a tracer dose, followed by unlabelled ligand and ligand of low SA) to determine which solution best describes the data [12].

We also applied three injections in our experimental protocol, which varied with respect to the amount of additional unlabelled ligand. Three different protocols were studied: (1) high SA – low SA – lower SA, (2) high SA – low SA – unlabelled and (3) high SA – unlabelled – low SA.

Although the different injection protocols displayed no systematic differences in the parameter values (Table 2), the sensitivities to parameter changes differed markedly between the protocols. Initial analyses indicated that the second protocol, high SA – low SA – unlabelled, was most sensitive to changes in the parameters, especially the B_{max}. Therefore, of the protocols investigated we recommend this protocol to calculate B_{max} and K_D in future studies. It also represents a logical starting point for further protocol optimisation as proposed by Muzic et al. [10]. An additional benefit of this protocol is, of course, that it requires only one radiosynthesis and has the potential to be reduced to only two injections at different SAs with a total scanning time of 40 min. As such it may also reduce the need for motion correction, which may otherwise be essential for patient studies.

SA in multiple-injection protocols

Multiple-injection PET studies to assess receptor density were originally analysed using a model which describes only the kinetics of the labelled ligand [19, 20]. This model was extended by Delforge et al., and now relies on explicit compartments for description of the kinetics of both labelled and unlabelled radioligand, which requires the solution of twice as many equations [9, 12, 21]. The main difference between these two models is the way they treat unlabelled ligand. The first model uses an analytical expression for SA, which applies only to the plasma and is an approximation for the bound compartment. In contrast, the second model accounts continuously for SA in each compartment. When administering more than one injection, the SA becomes a complex function of time that differs for each compartment. As a consequence, the SA calculated in plasma does not necessarily represent that in the bound compartment. The model with explicit compartments for labelled and unlabelled ligand therefore provides a more realistic prediction of the SA in the bound compartment. The preference for the second model was also demonstrated by Morris et al., who showed that the first model is unreliable because it may give non-physiological changes in receptor availability and B_{max} values with great uncertainties (error 30%–60%) [18].

In the present study the Delforge model was also chosen for analysis of PET receptor data with multiple injections. In Fig. 7 the log SA was plotted against time for each compartment. This figure clearly demonstrates that

the function of SA is very complicated, owing to the persistence of ligand in each compartment from previous injections, which contributes to SA thereafter. Furthermore, the function of SA in plasma does not resemble the function of SA at the point of interest, the bound compartment. These observations confirm the necessity of describing the SA in the bound compartment separately.

Reaction volume; apparent K_D

PET data are expressed in quantities per unit tissue volume. However, the true *local* concentration in any point cannot be measured in vivo because of the limited resolution of the PET camera and the internal heterogeneity of the tissue. To account for the heterogeneity of the tissue, an additional parameter, the reaction volume (V_R), was introduced.

The V_R can be estimated from the affinity measured in vitro, and the apparent affinity in vivo ($K_{D\ in\ vitro} = K_{D\ in\ vivo} \times V_R$). Moreover, the lipophilicity of the compound also provides information about the ligand distribution in tissue. Since (*S*)-CGP 12388 is a hydrophilic compound (log P = –0.6), it can be expected to distribute according to the fraction of extracellular fluid in tissue [14]. This assumption leads to a V_R of 0.15 for (*S*)-[^{11}C]CGP 12388, as has previously been demonstrated for other hydrophilic ligands [22, 23], including MQNB [13].

The in vivo affinity of (*S*)-CGP 12388 for the β-adrenoceptor in the myocardium measured in this study amounted to 0.58±0.22 n*M*, when corrected for a V_R of 0.15. This corresponds favourably with the K_D of CGP 12177 (0.33 n*M* for β_1 and 0.9 n*M* for β_2), as determined in rat cardiac microsomes [24].

The use of V_R is especially important in pathological conditions, since distribution volumes in these conditions may be significantly different from those in healthy tissues. For example, in transplantation patients, heart oedema results in an increased fraction of extracellular fluid. This has previously been confirmed with MQNB in transplanted patients, who had smaller $K_D V_R$ values than healthy volunteers, not because of changes in K_D but because of an increased V_R [25].

Estimation of B_{max}

β-Adrenoceptor densities, estimated in the whole left ventricle, amounted to 9.74±1.80 n*M*. These values correspond well with the range of cardiac β-adrenoceptor densities found in healthy volunteers using (*S*)-[^{11}C]CGP 12177 and the graphical method: 8.3–11.50 n*M* [3, 4, 5, 26, 27, 28, 29]. Moreover, they correspond fairly well with the 40–86 fmol/mg protein that Brodde found in vitro [30, 31], considering that tissue consists of approximately 10% protein.

The regional distribution of the β-adrenoceptor density in the left ventricle appeared to be heterogeneous, with relatively large amounts of receptors in the inferior wall, as compared with the anterior wall (Fig. 6). This phenomenon was consistent in all four volunteers (volunteers 3–6). Similarly, when using (*S*)-[^{11}C]CGP 12177, higher β-adrenoceptor densities were observed in the inferior wall of some of the healthy subjects and HCM patients studied [32]. In contrast, other researchers found a uniform distribution of β-adrenoceptors throughout the left ventricle with (*S*)-[^{11}C]CGP 12177, both in healthy controls and in subjects with HCM [3, 32]. A heterogeneous distribution of β-adrenoceptors was also observed in homogenates of anterior and inferior segments of the left ventricle, both in patients [33] and in dogs [34]. In these studies, however, a more pronounced β-adrenoceptor density was observed in the anterior wall as compared with the inferior wall, which is not surprising since anterior myocardial infarction results in greater depression of left ventricular performance than does inferior infarction [35]. Because of these equivocal observations, the validity of the heterogeneity found in the present study remains to be examined, in particular considering the potential disturbing effects of spill-over (e.g. from the liver) and signal loss due to the partial volume effect (e.g. septal wall of the myocardium). Once the contribution of these effects has been clarified, parametric polar mapping may become a valuable tool for investigating the regional distribution of β-adrenoceptors in the myocardium of both patients and healthy subjects.

Conclusion

Tracer kinetic modelling allows the estimation of all model parameters of the β-adrenergic radioligand (*S*)-[^{11}C]CGP 12388. In healthy volunteers, B_{max} and K_D were reliably calculated in the whole left ventricle (9.74±1.80 n*M* and 0.58±0.22 n*M*, respectively) and regional differences could be plotted in a parametric polar map (120 different segments). The protocol with high SA – low SA – unlabelled injections is to be preferred since this is the protocol most sensitive to changes in B_{max}. We conclude that (*S*)-[^{11}C]CGP 12388 in combination with a tracer kinetic method is useful for calculating regional B_{max} values in human left ventricle in vivo and may serve as a gold standard.

Acknowledgements. P. Doze was financially supported by the Netherlands Organisation for Scientific Research (NWO).

References

1. Michel MC, Brodde OE, Insel PA. Peripheral adrenergic receptors in hypertension. *Hypertension* 1990; 16:107–120.
2. Minneman KP, Hegstrand LR, Molinoff PB. Simultaneous determination of beta-1 and beta-2-adrenergic receptors in tissues containing both receptor subtypes. *Mol Pharmacol* 1979; 16:34–46.
3. Lefroy DC, De Silva R, Choudhury L, et al. Diffuse reduction of myocardial beta-adrenoceptors in hypertrophic cardiomyopathy: a study with positron emission tomography. *J Am Coll Cardiol* 1993; 22:1653–1660.
4. Merlet P, Delforge J, Syrota A, Angevin E, Maziere B, Crouzel C, Valette H, Loisance D, Castaigne A, Rande JL. Positron emission tomography with ^{11}C CGP-12177 to assess beta-adrenergic receptor concentration in idiopathic dilated cardiomyopathy. *Circulation* 1993; 87:1169–1178.
5. Qing F, Rahman SU, Rhodes CG, Hayes MJ, Sriskandan S, Ind PW, Jones T, Hughes JM. Pulmonary and cardiac beta-adrenoceptor density in vivo in asthmatic subjects. *Am J Respir Crit Care Med* 1997; 155:1130–1134.
6. Delforge J, Syrota A, Lancon JP, Nakajima K, Loc'h C, Janier M, Vallois JM, Cayla J, Crouzel C. Cardiac beta-adrenergic receptor density measured in vivo using PET, CGP 12177, and a new graphical method. *J Nucl Med* 1991; 32:739–748.
7. Boullais C, Crouzel C, Syrota A. Synthesis of 4-(3-*t*-butylamino-2-hydroxypropoxy)-benzimidazol-2(^{11}C)-one (CGP12177). *J Label Comp Radiopharm* 1986; 23:565–567.
8. Mintun MA, Raichle ME, Kilbourn MR, Wooten GF, Welch MJ. A quantitative model for the in vivo assessment of drug binding sites with positron emission tomography. *Ann Neurol* 1984; 15:217–227.
9. Delforge J, Syrota A, Mazoyer BM. Experimental design optimisation: theory and application to estimation of receptor model parameters using dynamic positron emission tomography. *Phys Med Biol* 1989; 34:419–435.
10. Muzic RF Jr, Saidel GM, Zhu N, Nelson AD, Zheng L, Berridge MS. Iterative optimal design of PET experiments for estimating beta-adrenergic receptor concentration. *Med Biol Eng Comput* 2000; 38:593–602.
11. Elsinga PH, van-Waarde A, Jaeggi KA, Schreiber G, Heldoorn M, Vaalburg W. Synthesis and evaluation of (*S*)-4-(3-(2′-[^{11}C]isopropylamino)-2-hydroxypropoxy)-2H-benzimidazol + ++-2-one ((*S*)-[^{11}C]CGP 12388) and (*S*)-4-(3-((1′-[^{18}F]-fluoroisopropyl)amino)-2-hydroxypropoxy)-2H-+++benzimidazol-2-one ((*S*)-[^{18}F]fluoro-CGP 12388) for visualization of beta-adrenoceptors with positron emission tomography. *J Med Chem* 1997; 40:3829–3835.
12. Delforge J, Syrota A, Mazoyer BM. Identifiability analysis and parameter identification of an in vivo ligand-receptor model from PET data. *IEEE Trans Biomed Eng* 1990; 37: 653–661.
13. Delforge J, Syrota A, Bendriem B. Concept of reaction volume in the in vivo ligand-receptor model [see comments]. *J Nucl Med* 1996; 37:118–125.
14. Walker JL. Intracellular inorganic ions in cardiac tissue. In: Fozzard H, Haber E, Jennings R, Katz AM, Morgan HE, eds. *The heart and cardiovascular system, scientific foundations.* New York: Raven Press; 1986:561–572.
15. Coleman TF, Li Y. An interior, trust region approach for nonlinear minimization subject to bounds. *SIAM J Optimization* 1996; 6:418–445.
16. Coleman TF, Li Y. On the convergence of reflective Newton methods for large-scale nonlinear minimization subject to bounds. *Math Programming* 1994; 67:189–224.
17. Millet P, Delforge J, Pappata S, Syrota A, Cinotti L. Error analysis on parameter estimates in the ligand-receptor model: application to parameter imaging using PET data. *Phys Med Biol* 1996; 41:2739–2756.
18. Morris ED, Alpert NM, Fischman AJ. Comparison of two compartmental models for describing receptor ligand kinetics and receptor availability in multiple injection PET studies. *J Cereb Blood Flow Metab* 1996; 16:841–853.
19. Huang SC, Bahn MM, Barrio JR, Hoffman JM, Satyamurthy N, Hawkins RA, Mazziotta JC, Phelps ME. A double-injection technique for in vivo measurement of dopamine D2-receptor density in monkeys with 3-(2′-[^{18}F]fluoroethyl)spiperone and dynamic positron emission tomography. *J Cereb Blood Flow Metab* 1989; 9:850–858.
20. Bahn MM, Huang SC, Hawkins RA, Satyamurthy N, Hoffman JM, Barrio JR, Mazziotta JC, Phelps ME. Models for in vivo kinetic interactions of dopamine D2-neuroreceptors and 3-(2′-[^{18}F]fluoroethyl)spiperone examined with positron emission tomography. *J Cereb Blood Flow Metab* 1989; 9:840–849.
21. Delforge J, Syrota A, Bottlaender M, Varastet M, Loc'h C, Bendriem B, Crouzel C, Brouillet E, Maziere M. Modeling analysis of [^{11}C]flumazenil kinetics studied by PET: application to a critical study of the equilibrium approaches. *J Cereb Blood Flow Metab* 1993; 13:454–468.
22. Carson RE, Channing MA, Blasberg RG, Dunn BB, Cohen RM, Rice KC, Herscovitch P. Comparison of bolus and infusion methods for receptor quantitation: application to [^{18}F]cyclofoxy and positron emission tomography. *J Cereb Blood Flow Metab* 1993; 13:24–42.
23. Gjedde A, Wong DF. Modeling neuroreceptor binding of radioligands in vivo. In: Frost JJ, Wagner HN Jr. *Quantitative imaging: neuroreceptors, neurotransmitters and enzymes.* New York: Raven Press; 1990:51–79.
24. Nanoff C, Freissmuth M, Schutz W. The role of a low beta 1-adrenoceptor selectivity of [^{3}H]CGP-12177 for resolving subtype-selectivity of competitive ligands. *Naunyn Schmiedebergs Arch Pharmacol* 1987; 336:519–525.
25. Le Guludec D, Delforge J, Syrota A, Desruennes M, Valette H, Gandjbakhch I, Merlet P. In vivo quantification of myocardial muscarinic receptors in heart transplant patients. *Circulation* 1994; 90:172–178.
26. Choudhury L, Rosen SD, Lefroy DC, Nihoyannopoulos P, Oakley CM, Camici PG. Myocardial beta adrenoceptor density in primary and secondary left ventricular hypertrophy. *Eur Heart J* 1996; 17:1703–1709.
27. De Silva R, Choudhury L, Lefroy DC, Uren NG, Rhodes CG, Hughes JMB, Jones T, Camici PG. Non-invasive regional assessment of human cardiac beta adrenoceptors (bAR) [abstract]. *Circulation* 1992; 86:I-298.
28. Rosen SD, Boyd H, Rhodes CG, Kaski JC, Camici PG. Myocardial beta-adrenoceptor density and plasma catecholamines in syndrome X. *Am J Cardiol* 1996; 78:37–42.
29. Qing F, Rhodes CG, Hayes MJ, Krausz T, Fountain SW, Jones T, Hughes JM. In vivo quantification of human pulmonary beta-adrenoceptor density using PET: comparison with in vitro radioligand binding. *J Nucl Med* 1996; 37:1275–1281.
30. Brodde OE, Karad K, Zerkowski HR, Rohm N, Reidemeister JC. Coexistence of b1- and b2-adrenoceptors in human heart and lung [abstract]. *Br J Pharmacol* 1983; 78 (Suppl):72.

31. Brodde OE. Beta1- and beta2-adrenoceptors in the human heart: properties, function and alterations in chronic heart failure. *Pharmacol Rev* 1991; 43:203–242.
32. de Jong RM, Rhodes CG, Anthonio RL, Willemsen AT, Blanksma PK, Lammertsma AA, Rosen SD, Vaalburg W, Crijns HJ, Camici PG. Parametric polar maps of regional myocardial beta-adrenoceptor density. *J Nucl Med* 1999; 40: 507–512.
33. Ungerer M, Hartmann F, Karoglan M, Chlistalla A, Ziegler S, Richardt G, Overbeck M, Meisner H, Schomig A, Schwaiger M. Regional in vivo and in vitro characterization of autonomic innervation in cardiomyopathic human heart. *Circulation* 1998; 97:174–180.
34. Burnam MH, Sethna DH, Rose DM, Stern CS, Shell WE. Differences in beta-adrenoceptor binding in anterior and inferior myocardial wall microsomes of normal canine left ventricle. *Cardiovasc Res* 1981; 15:239–244.
35. Miller RR, Olson HG, Vismara LA, Bogren HG, Amsterdam EA, Mason DT. Pump dysfunction after myocardial infarction: importance of location, extent and pattern of abnormal left ventricular segmental contraction. *Am J Cardiol* 1976; 37:340–344.